JACS
JOURNAL OF THE AMERICAN CHEMICAL SOCIETY

Article

pubs.acs.org/JACS

Effect of Metal Complexation on the Conductance of Single-Molecular Wires Measured at Room Temperature

Julia Ponce,[†,⊥] Carlos R. Arroyo,[‡,⊥] Sergio Tatay,[†] Riccardo Frisenda,[‡] Pablo Gaviña,[∥] Daniel Aravena,[§] Eliseo Ruiz,[§] Herre S. J. van der Zant,*[,‡] and Eugenio Coronado*[,†]

[†]Instituto de Ciencia Molecular (ICMol), Universidad de Valencia, Catedrático José Beltrán 2, 46980 Paterna, Spain

[‡]Kavli Institute of Nanoscience, Delft University of Technology, Lorentzweg 1, 2628 CJ Delft, The Netherlands

[§]Departament de Química Inorgànica and Institut de Recerca de Química Teòrica i Computacional, Universitat de Barcelona, Diagonal 645, 08028 Barcelona, Spain

[∥]Centro de Reconocimiento Molecular y Desarrollo Tecnológico (IDM), Unidad mixta Universidad Politécnica de Valencia-Universidad de Valencia, Dr. Moliner 50, 46100 Burjassot, Spain

Supporting Information

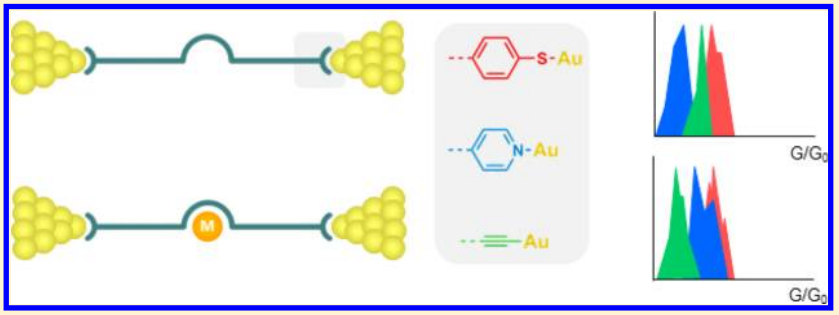

ABSTRACT: The present work aims to give insight into the effect that metal coordination has on the room-temperature conductance of molecular wires. For that purpose, we have designed a family of rigid, highly conductive ligands functionalized with different terminations (acetylthiols, pyridines, and ethynyl groups), in which the conformational changes induced by metal coordination are negligible. The single-molecule conductance features of this series of molecular wires and their corresponding Cu(I) complexes have been measured in break-junction setups at room temperature. Experimental and theoretical data show that no matter the anchoring group, in all cases metal coordination leads to a shift toward lower energies of the ligand energy levels and a reduction of the HOMO−LUMO gap. However, electron-transport measurements carried out at room temperature revealed a variable metal coordination effect depending on the anchoring group: upon metal coordination, the molecular conductance of thiol and ethynyl derivatives decreased, whereas that of pyridine derivatives increased. These differences reside on the molecular levels implied in the conduction. According to quantum-mechanical calculations based on density functional theory methods, the ligand frontier orbital lying closer to the Fermi energy of the leads differs depending on the anchoring group. Thereby, the effect of metal coordination on molecular conductance observed for each anchoring could be explained in terms of the different energy alignments of the molecular orbitals within the gold Fermi level.

INTRODUCTION

The research field of single-molecule electronics emerged with the aim of using tailored individual molecules as electronic building blocks.[1] Among other molecular systems, the integration of functional metal complexes in electronic circuits has attracted particular interest because of the additional exciting prospects offered by the possibility of controlling and manipulating metal redox and spin states at the molecular level.[2−4] On that basis, metal-containing molecular devices capable of acting as molecular-based switches or memories have been proposed.[2−7] Moreover, several studies of charge transport through single-molecule junctions[4,8−11] have reported a broad variety of quantum phenomena triggered by the presence of a metal ion in the conduction pathway. Of special relevance is the Kondo resonance observed for a single Co(II) complex embedded in an electromigrated break junction.[9] Recent studies have also stated that the existence of high permanent dipole moments in single transition-metal complexes can lead to current-rectification behavior.[5,6]

In single-molecule electronics it is customary to functionalize the target molecules with suitable anchoring groups in order to improve the electron transport and mechanical stability. In the particular case of metal complexes, on the basis of the location of the anchoring groups, the molecular structures can fall into two categories. In the first one, represented in Figure 1 A, the anchoring groups are placed in two separate ligands. Hence, when contacted, the charge current is forced to pass through

Received: February 13, 2014

   dx.doi.org/10.1021/ja5012417 | J. Am. Chem. Soc. XXXX, XXX, XXX−XXX

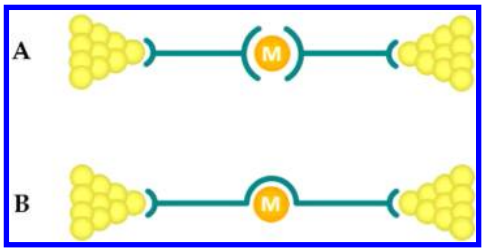

Figure 1. Schematic representations of metallic complexes in single-molecule junction configurations: (A) metal-complex junction with the two anchoring groups located in different ligands; (B) metal-complex junction in which the two anchoring groups are located in the same ligand.

the metal ion, and in the absence of the metal center the molecule breaks down.[2,4,8−11] Figure 1 B illustrates the second category, in which the anchoring groups are placed at both ends of the same ligand. In this case, current flows through the ligand even in the absence of the metal ion. This approach is particularly interesting since it offers the possibility to investigate electron transport in either the presence or the absence of a metal center, enabling the study of the metal coordination effect.

As far as we know, this kind of study has been performed only on peptides[12] and ligands of the 2,2′-bipyridine family.[5,6,13] All of these compounds showed an increase in molecular conductance upon coordination, which in the case of bipyridines was attributed to the increased conjugation derived from the planar configuration adopted by the bipyridine unit in the metal chelate. This explanation is supported by several detailed studies of functionalized biphenyls, in which the conductance showed a $\cos^2 \Phi$ dependence on the torsion angle between the phenyl rings (Φ).[14−16] Therefore, in this scenario the effect of metal coordination is obscured by changes in the geometry. Because of this, with the aim of isolating the effect of metal coordination on the conductance of molecular wires, in the present work we investigated the single-molecule electron transport properties of a series of rigid ligands and their corresponding Cu(I) complexes. For that purpose, we designed a series of molecular wires bearing a 1,10-phenanthroline (phen) metal-binding site and end-substituted with different anchoring groups (see Figure 2). Both phens and 2,2′-bipyridines are considered excellent coordination chelates capable of forming stable complexes with most transition-metal ions. However, in phens the torsional degree of freedom is suppressed, and the imine nitrogens are fixed in a cis conformation even before interaction with the metal. On that basis, any change in the conductance of our phen-based molecular wires upon metal chelation must be directly derived from the effect of the metal, with minor contributions coming from changes in molecular conformation.

In a first set of experiments, with the aim of systematically studying the effect of the anchoring groups on the electron transport properties, we synthesized a series of phenanthroline-based molecular backbones functionalized with thiol (**1**), pyridine (**2**), and acetylene (**3**) anchoring groups (Figure 2). It is well-known that the anchoring groups affect the electron transport through molecular wires.[17−19] To date, thiols have been the favorite choice in electron transport studies because of the strong covalent bond formed between sulfur and gold atoms.[20] In these experiments, the use of protected thiols was mandatory since in solution they suffer from spontaneous oxidative dimerization to disulfides.[20] The acetylthio (AcS)

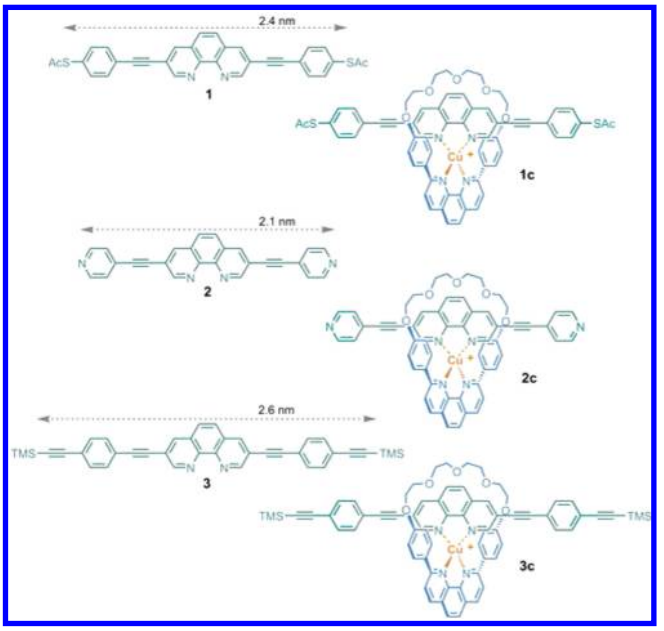

Figure 2. Chemical structures of molecular wires **1**−**3** and complexes **1c**−**3c**. The molecular lengths were calculated from DFT-optimized structures.

group has been demonstrated to be a very appropriate protecting group because it is resistant to Pd-catalyzed coupling conditions and can be easily cleaved in the presence of gold electrodes even without the assistance of any deprotecting agent.[21] In addition to thiols, although their use is not so extended, terminal para-substituted pyridines have proved to be promising linkers in molecular electronics.[19] Several studies have revealed that pyridyls form very stable contacts in which molecules adopt particularly well-defined binding geometries between the leads, thus affording more reproducible conductance values than the aforementioned thiols.[19,22,23] From the chemical point of view, the use of pyridine derivatives is very advantageous since they do not need to be protected and are compatible with a wide variety of reaction conditions. More recently, the formation of direct Au−C covalent bonds, starting from either trimethyltin ($SnMe_3$, TMT) methylenes or trimethylsilyl ($SiMe_3$, TMS) acetylenes, has been explored in the study of molecular conductance.[24−26] When TMS or TMT groups are cleaved off on gold surfaces with (TMS) or without (TMT) the assistance of a chemical agent, a σ bond between gold and a carbon atom is formed. In the case of TMT methylenes, these anchorings have given rise to conductance values up to 100 times larger than those for the analogous oligophenyl molecules with amine terminations.[25]

In a second phase, we studied the effect of Cu(I) coordination on the conductance of wires **1**, **2**, and **3**. Copper complexes have been widely studied in coordination chemistry, and they attract special interest since they possess two available oxidation states, I and II, with very different magnetic and spectroscopic properties.[27]

The single-molecule conductance features at room temperature reported herein were investigated using the mechanically controlled break junction (MCBJ) technique in the low-bias regime. Furthermore, we employed a new junction-formation method, the so-called self-breaking (SB) technique.[28] This method turned out to be well-suited for the evaluation of the transport properties of bulky copper complexes **1c**−**3c**.

dx.doi.org/10.1021/ja5012417 | J. Am. Chem. Soc. XXXX, XXX, XXX−XXX

Coordination to Cu(I) ion led to different changes in the conductance depending on the anchoring group used, which will be rationalized in terms of electronic and density functional theory (DFT) considerations.

EXPERIMENTAL SECTION

Chemical Synthesis. The chemicals and solvents used were purchased from commercial sources and used without further purification, unless specially mentioned. Detailed synthetic procedures and characterization data for the compounds described herein are included in the Supporting Information (S.I.).

Spectrochemical Methods. ^{1}H NMR spectra were acquired on a Bruker AVANCE DRX 300 spectrometer. The spectra were referred to residual solvent proton references.[29] Electrospray mass spectrometry [MS(ES)] was performed using a Waters Micromass ZQ spectrometer in the positive ion mode. Absorption spectra were recorded in dichloromethane solution at a concentration of 1×10^{-5} M on a Shimadzu UV-2501PC spectrophotometer using 1 cm path length quartz cuvettes.

Electrochemistry. Electrochemical measurements were performed in a nitrogen glovebox using an Autolab PGSTAT 128N potentiostat and a three-electrode electrochemical cell consisting of a glassy carbon working electrode, a platinum wire counter electrode, and a silver wire pseudoreference electrode. $[Cu(dmp)_2](PF_6)$ (dmp = 2,9-dimethyl-phenanthroline) was used as reference (0.64 V vs SCE in dichloromethane).[30] Supporting electrolyte solutions were prepared from anhydrous dichloromethane and tetrabutylammonium hexafluorophosphate ($TBAPF_6$).

Deposition of the Conjugated Molecular Wires onto the Electrodes. In the experiments reported here, the molecules were deposited onto the MCBJ devices by pipetting 2 μL of a freshly prepared 0.5 mM solution. In the case of **1** and **3**, 1 equiv of tetrabutylammonium hydroxide (TBAOH) or tetrabutylammonium fluoride (TBAF) was added to the solution just before the deposition to help with the deprotection of the AcS and TMS groups, respectively. The solvents used for the different backbones were dichlorobenzene for **1**, dichloromethane for **2**, and a 1:4 mixture of tetrahydrofuran and octane in the case of **3**. For the Cu(I) complexes **1c**−**3c**, dichloromethane was used as the solvent. Moreover, in the case of the complexes **1c**−**3c**, 10 equiv of hydrazine in THF was added to the solution just before the deposition to prevent oxidation to Cu(II). Finally, after the solvent had dried over the electrode, a vacuum can was placed, and the sample was pumped down to around 10^{-6} mbar for approximately 1 h before the start of the experiment.

Conductance Measurements. Single-molecule conductance measurements were carried out at room temperature using the MCBJ technique.[31] Briefly, the device consists of a narrow gold bridge suspended above a flexible substrate. This device is clamped in a three-point bending configuration, as schematically shown in Figure 3. After the deposition of the molecules from solution under ambient conditions, the suspended gold bridge is stretched by driving the pushing rod against the bottom part of the MCBJ device until it breaks, leaving a pair of atomically sharp electrodes. Once the bridge is broken for the first time, atomic-sized contacts can be repeatedly formed and broken by moving the electrodes toward and away from each other. During the whole process, the conductance $G = I/V$ is simultaneously measured by applying a bias voltage of 0.1 V across the electrodes. During the breaking process, the conductance decreases in a stepwise fashion. Just before the complete rupture of the gold wire, the conductance usually exhibits a plateau that is nearly flat and very close to G_0, where G_0 is the conductance quantum ($G_0 = 2e^2/h$, where e is the elementary charge and h is Planck's constant). This plateau characterizes the formation of a contact consisting of a single gold atom bridging the gap between the electrodes. Upon further stretching, the contact breaks and the conductance drops abruptly to a value of 10^{-3}−$10^{-4}G_0$. Beyond this point, electron tunneling between the electrodes leads to an exponential conductance decay as a function of the electrode displacement. The abrupt drop in conductance after the breaking of the one-atom contact is associated with mechanical relaxation and atomic rearrangements at the electrode apexes.[32] When a molecule is trapped between the electrodes, conductance plateaus can be observed for long electrode displacements. After the contact rupture, the electrodes are fused together to give a conductance value around $80G_0$ to ensure the formation of clean gold contacts.

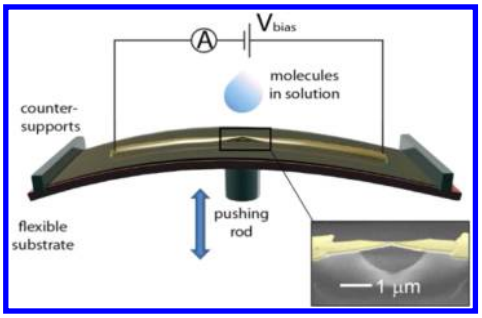

Figure 3. Layout of the experimental setup. Inset: scanning electron micrograph of a device.

Alternatively, a variation of the traditional MCBJ experiment, the self-breaking method, was used to form molecular junctions.[28] This method has been previously used to investigate the stability of atomic gold contacts. In these experiments, the junction is first stretched by bending the substrate with a bias voltage of 0.1 V applied across the electrodes. Once the conductance of the junction reaches a value below $10G_0$ (typically $6G_0$), the bending process is stopped and the conductance is continuously monitored as a function of time. As a result of the high mobility of gold atoms at room temperature, the junction breaks by itself. When the conductance drops below a minimum conductance value ($G < 10^{-7}G_0$), the electrodes are fused together again to give a conductance of $80G_0$, and a new SB trace is started. The key point of this technique is that when no molecules are present, the time interval over which the conductance falls from G_0 to $10^{-7}G_0$ is short (typically less than 100 s). However, when sample molecules are present, conductance plateaus can be observed for long periods of time, even several hours. These plateaus are indicative of the presence of the target molecules trapped between the electrodes. We define the junction lifetime as the time required for the conductance to drop from $G = G_0$ to $G < 10^{-7}G_0$. Considering that the lifetimes measured for pure solvent molecules are typically below 100 s (see the S.I.), we can assume that molecular junctions are formed when the junction lifetime exceeds 100 s, and hence, a trapping probability can be calculated.

Computational Studies. DFT calculations on the isolated molecules were performed employing the B3LYP functional[33] and the TZV basis set, as implemented in the Gaussian09 software package.[34] Nonequilibrium Green's function plus DFT (NEGF+DFT) calculations were carried out by means of the TranSIESTA[34] routine included in SIESTA 3.1[35] using the PBE functional[36] and the DZP basis set for the molecule and the SZ basis set for the gold atoms. Device models consisted of two five-layer Au(111) electrodes bridged with gas-phase-optimized molecules. The adsorption sites and distances of the anchoring groups to the gold surface were chosen according to previous studies[37−39] to be the following: bridge site, 2.5 Å for **1**; atop site, 2.5 Å for **2**; atop site, 2.0 Å for **3**. Copper-coordinated models preserved the adsorption geometry of the corresponding backbones.

RESULTS AND DISCUSSION

Design and Synthesis. As previously mentioned, we were interested in evaluating the effect of metal coordination on the conductance of molecular wires while avoiding as much as possible the contribution derived from structural or geometrical distortions. For that purpose, we chose rigid phen as the coordination unit. In order to symmetrically bind the phen moiety to the gold leads, we designed molecular wires **1**−**3**.

dx.doi.org/10.1021/ja5012417 | J. Am. Chem. Soc. XXXX, XXX, XXX−XXX

The wires are formed by a central phen moiety substituted at the 3 and 8 positions with suitable conjugated anchoring groups (Figure 2). As anchoring groups we used *p*-arylethynyl spacers functionalized with −SAc (**1**), pyridine (**2**) and ethynyl-TMS (**3**) terminations.

The syntheses of molecular wires **1**−**3** are summarized in Scheme 1. The preparation of **1** and **2** has been already

Scheme 1. Synthesis of Molecular Wires 1−3[a]

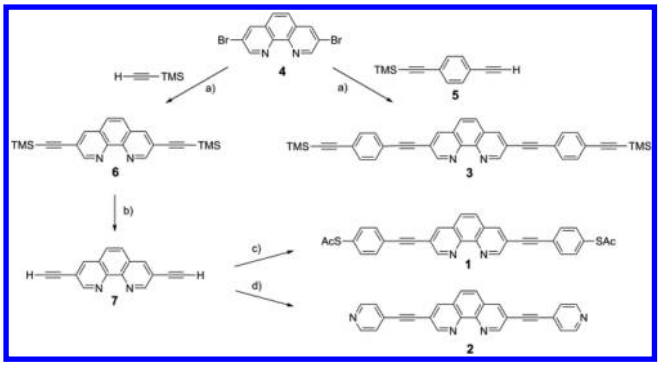

[a]Reagents and conditions: (a) $Pd(PPh_3)Cl_2$, CuI, THF, i-Pr_2NH (74% for **6**, 50% for **3**); (b) K_2CO_3, MeOH (97%); (c) *S*-(4-iodophenyl)-ethanethiolate (2 equiv), $Pd(dba)_2$, PPh_3, CuI, THF, DIEA (40%); (d) 4-iodopyridine (2 equiv), $Pd(PPh_3)_4$, CuI, THF, DIEA (84%).

reported[40,41] and their syntheses were accomplished following a slight modification of the described synthetic procedures. In short, the phen core was symmetrically grown by the coupling of 3,8-dibromo-1,10-phenanthroline (**4**)[42] with commercial ethynyltrimethylsilane to give **6** followed by desilylation under basic conditions (Na_2CO_3 in methanol) to afford diethynyl intermediate **7** in high yield.[43] Final coupling with 2 equiv of 1-(*S*-acetylthio)-4-iodobenzene or 4-iodopyridine under Sonogashira conditions afforded the desired molecular rods **1** and **2**, respectively. The yield of **1** was enhanced by the use of the $Pd(dba)_2$ catalyst in the last step of the synthesis, as described by Flatt et al.[44] The synthesis of compound **3**, which is reported here for the first time, was carried out by the coupling of **4** with 2 equiv of ((4-ethynylphenyl)ethynyl)trimethylsilane (**5**) under the same coupling conditions as used in the case of **6**. Compound **5** had been previously prepared by the reaction of 1,4-diethynylbenzene with *n*-BuLi and subsequent quenching of the lithium intermediate by the addition of chlorotrimethylsilane.[45]

The synthesis of the threaded copper complexes **1c**−**3c** (depicted in Scheme 2) was carried out by mixing equimolar amounts of macrocycle **M** and $[Cu(CH_3CN)_4]PF_6$ with the corresponding molecular backbones **1**−**3**. Cu(I) and phen ligands form tetrahedral complexes that are kinetically labile.

Scheme 2. Copper-Templated Self-Assembly of Complexes 1c−3c

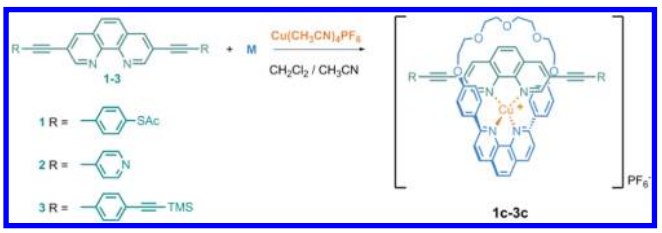

Despite this, the 2,9-aryl substituents in macrocycle **M**[46] provide a very stable coordination environment for Cu(I) ions and minimize metal exchange,[47] and the closed nature of **M** avoids the formation of the homoleptic $Cu(\mathbf{M})_2$ complex. For these reasons, the combination of Cu(I) ions with our 3,8-substituted molecular backbones **1**−**3** and macrocycle **M** in a 1:1:1 stoichiometry assures the selective formation of the heteroleptic $Cu(\mathbf{M})(\mathbf{1}-\mathbf{3})$ complexes.[48]

The formation of the interlocked species was evidenced by the rapid appearance of a red-brown color characteristic of Cu(I) complexes with two aromatic diimine ligands[49,50] and was further verified by ^{1}H NMR and MS(ES) analyses. The C_{2v} symmetry of the complexes was evidenced by ^{1}H NMR analyses, since all of the signals in the spectra integrated to at least 2H.

Photo- and Electrochemical Characterization. Organic backbones **1**−**3** and their respective Cu(I) complexes **1c**−**3c** were further characterized by means of UV−vis spectroscopy and cyclic voltammetry. As can be observed in the UV−vis spectra (see S.I. Figure 1), the organic backbones **1**−**3** present very intense absorption bands (ε > 50 000 M^{-1} cm^{-1}) around 285 and 345 nm arising from $\pi-\pi$ transitions.[51] Complexes **1c**−**3c** show additional weak broad bands (ε < 4000 M^{-1} cm^{-1}) in the region between 400 and 550 nm associated with metal-to-ligand charge transfer (MLCT) processes arising from the presence of the metal atom.[50,52]

The cyclic voltammograms of molecular backbones **1**−**3** present a single irreversible reduction process below −1.0 V (see S.I. Figure 2). In the corresponding Cu(I) complexes these irreversible reduction processes become somewhat more defined, and reduction peaks can be observed. Additionally, a quasi-reversible peak associated with the Cu(I/II) couple appears at around 0.5 V.[49]

We estimated the optical HOMO−LUMO gaps (E_g^{opt}) from the onsets of the lowest-energy bands in the UV−vis spectra. Moreover, according to the empirical relationship proposed by Forrest and co-workers,[53,54] we estimated the LUMO energies of **1**−**3** and **1c**−**3c** and also the HOMO energies and the HOMO−LUMO gaps (E_g^{elec}) of **1c**−**3c** from the onset of the reduction and oxidation waves. The results of these calculations and some other relevant data are summarized in Table 1. The optical data show a reduction of the HOMO−LUMO gap by more than 1.0 eV upon metal coordination. The E_g values show a good correlation between the experimental methods and DFT calculations on the isolated molecules, although the latter values are slightly overestimated.[55]

DFT Calculations. As a first approximation, we performed DFT calculations for the isolated backbone molecules **1**−**3** and those after the formation of the Cu(I) complexes **1c**−**3c**. The reduction of the gap in the copper complexes with respect to the backbones is well-reproduced in the calculations, with the calculated values being slightly higher, as shown in Table 1. Besides, the coordination of Cu(I) results in a general shift of the frontier orbitals of the three backbones to lower energies (Figure 4). This trend is consistent with the inclusion of a positively charged fragment that withdraws some electron density from the backbone, and similar trends have been observed before upon metal coordination of conjugated wires.[55]

Electrical Characterization. *Conductance Histograms of Backbone Molecules 1−3 Obtained by the MCBJ Method.* As described in the Experimental Section, we collected thousands of breaking traces by measuring the conductance as a function of electrode displacement (z) with a bias voltage of 0.1 V

dx.doi.org/10.1021/ja5012417 | J. Am. Chem. Soc. XXXX, XXX, XXX−XXX

Table 1. Electrochemical and Optical Properties of 1−3 and 1c−3c

	$E_{1/2}^{red}$ (V)[a]	$E_{1/2}^{ox}$ (V)[a]	E_{HOMO}(eV)[b]	E_{LUMO} (eV)[b]	E_g^{elec} (eV)[c]	λ_{max} (nm)	E_g^{opt} (eV)[d]	E_g^{DFT} (eV)[e]
1	−1.67	–	–	−2.16	–	384	3.23	3.43
2	−1.60	–	–	−2.21	–	371	3.34	3.65
3	−1.10	–	–	−3.64	–	393	3.15	3.45
1c	−1.67	0.54	−4.35	−2.38	1.97	596	1.80	2.64
2c	−1.52	0.52	−4.25	−2.38	1.88	612	1.91	2.50
3c	−1.28	0.181	−4.84	−3.35	1.40	510	1.70	2.59

[a] $E_{1/2}$ values in V vs SCE recorded in CH_2Cl_2 with $TBAPF_6$ as the supporting electrolyte. The concentration was 1 mM, and the scan rate 100 mV/s. [b] The HOMO and LUMO energies were determined from the onsets of the first oxidation wave and the first reduction wave in cyclic voltammograms. [c] The electrochemical HOMO−LUMO gap is defined as $E_g^{elec} = -(E_{HOMO} - E_{LUMO})$. [d] Optical HOMO−LUMO gaps were determined from the onsets of the lowest-energy visible absorption bands. [e] Calculations were performed using DFT at the B3LYP/TZV level. In each case, the onset was calculated as the intersection between the baseline and a tangent line that touches the point of inflection.

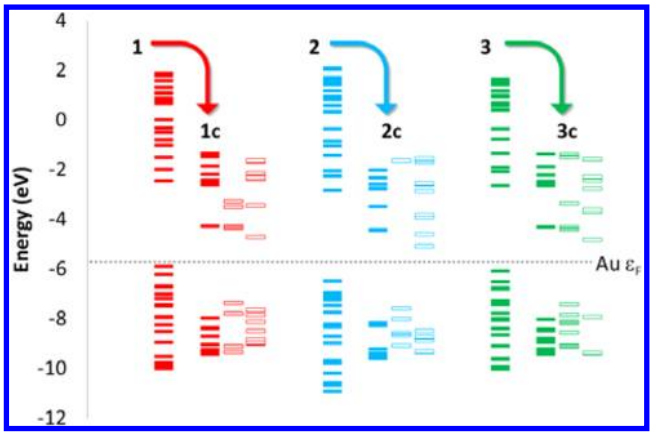

Figure 4. Orbital energy level diagram showing the stabilization of the backbones (**1**−**3**) upon Cu(I) coordination (**1c**−**3c**). Colored rectangles correspond to backbone levels, empty rectangles to copper centers and macrocycle orbitals, and weakly colored rectangles to mixed copper/macrocycle-backbone levels. The Fermi level corresponding to the bulk gold phase (−5.53 eV) is presented for reference.

applied across the electrodes; for these settings, the noise level in our setup was close to $1 \times 10^{-6} G_0$. In comparison with the empty gold junctions, individual breaking traces measured with electrodes exposed to pure solvents did not introduce additional features. By contrast, when the MCBJ devices were exposed to solutions containing the target molecules, additional conductance plateaus were observed for sub-G_0 conductance values (Figure 5 insets).

Typical trace histograms obtained from 1000 consecutive breaking traces measured in the presence of backbones **1**−**3** are shown in Figure 5. To build these two-dimensional trace histograms, the individual breaking traces without any data

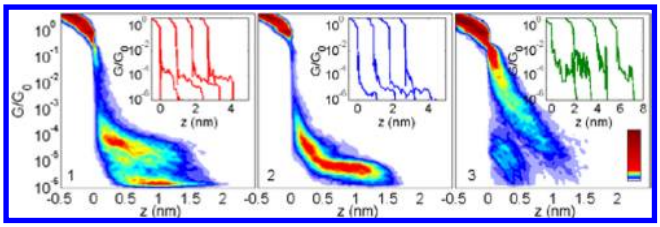

Figure 5. Trace histograms obtained from 1000 breaking traces such as those shown in the insets for junctions exposed to 0.5 mM solutions of **1**, **2**, and **3**. The bias voltage was 0.1 V, and the electrode displacement speed was 12 nm/s. The color scale indicates the number of counts found at each conductance value for a certain electrode displacement.

selection were shifted along the electrode displacement (horizontal) axis to fix the rupture of the one-atom gold contact at zero. The areas with high counts denote the most probable evolution during the formation of the molecular junctions. The histograms for **1** and **2** show the occurrence of conductance plateaus with distinguishable conductance values, but traces measured in the presence of **3** appear noisier. According to their length, the plateaus observed just after the breaking of the metallic contact correspond to the formation of single-molecule junctions, where the anchoring groups provide the mechanical and electrical connection between the gold electrodes and the individual molecule.[56] However, at shorter electrode displacements the phen unit may compete with the terminal anchoring groups and contribute to the conductance.[57−59]

Figure 6 shows the one-dimensional (1D) conductance histograms obtained for **1**−**3** from the data in Figure 5. The 1D

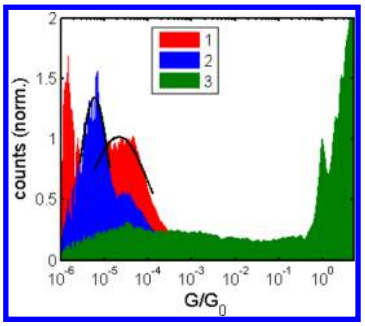

Figure 6. One-dimensional conductance histograms obtained from the trace histograms displayed in Figure 5. The most probable conductance values were obtained from Gaussian fits of the conductance histograms (black lines).

conductance histograms reveal well-defined peaks only in the cases of **1** and **2**. In the case of **1**, a broad peak is centered around $2.1 \times 10^{-5} G_0$, while for molecule **2** the peak is centered around $5.8 \times 10^{-6} G_0$. Although single-molecule transport through thiolated bipyridyl oligo(phenylene ethynyl) (BPE) molecules has been studied before,[13,60] the authors did not report any low-bias conductance value for comparison. Nevertheless, backbone **1** exhibits a conductance value close to the value of $2.4 \times 10^{-5} G_0$ reported for the dithiolated biphenyl oligo(phenylene ethynyl) derivative by Zhang and coworkers.[61] As in the case of **1**, in this molecule the central aromatic rings are forced to remain planar through proper chemical substitution. Thus, the phen moiety affords a molecular resistance value comparable to that reported for a

dx.doi.org/10.1021/ja5012417 | J. Am. Chem. Soc. XXXX, XXX, XXX−XXX

planar biphenyl unit. In agreement with its molecular length, molecular backbone **2** presents a molecular conductance value intermediate between those reported for OAE3 and OAE4 [OAE = oligo(arylene ethylene)] with terminal pyridyl groups measured in MCBJ.[62] Previous works on tolane molecules using MCBJ reported by Hong and co-workers[19,26] observed an increase in the resistance in passing from acetylenes to thiols and then to pyridines [G(acetylenes) > G(thiols) > G(pyridines)] and described the following sequence for junction formation probability and stability: pyridines, acetylenes > thiols. In the present case, we observed a similar trend in conductance in passing from thiol to pyridine anchoring groups. However, under our experimental conditions, acetylenes did not afford well-defined conductance plateaus in the measured breaking traces (Figure 5).

*Conductance Histograms of **1c**–**3c** Obtained by the MCBJ Method.* The trace histograms obtained for junctions exposed to copper complexes **1c**–**3c** did not show horizontal regions of high counts at the same electrode displacement speed used in the backbone measurements (12 nm/s). This fact indicates a low probability of trapping a molecule between the electrodes. However, we observed that the occurrence of conductance plateaus increased considerably when the speed of electrode displacement was reduced. A possible explanation for the differences in the behaviors of the backbone molecules and the copper complexes could rely on the fact that the central ring, being so bulky, prevents the formation of molecular junctions when the electrodes are moved apart at high speed (Figure 7).

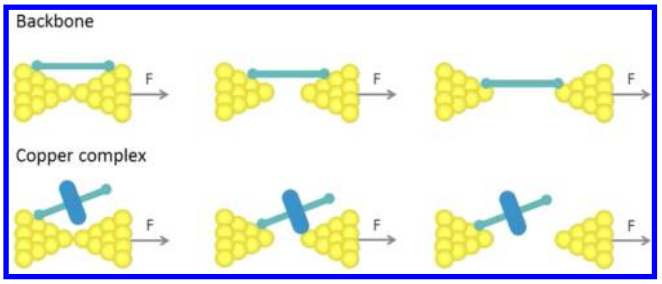

Figure 7. Sketches representing a possible explanation for the different trapping probabilities shown by the backbones and the copper complexes.

*Conductance Histograms of Backbone Molecules **1**–**3** Obtained by the SB Method.* By using the self-breaking method, we measured a total of 61, 336, and 139 self-breaking traces for **1**, **2**, and **3**, respectively. In contrast to the traditional MCBJ method, the SB approach consists of following the conductance evolution of atomic-sized contacts as a function of time rather than electrode displacement. Figure 8 shows the histograms recorded by measuring consecutive SB traces in the presence of backbones **1**–**3** without any data selection. To build these histograms, the individual SB traces were shifted along the time axis to fix the rupture of the one-atom gold contact at zero. In the case of pure solvent, the time that the junction has a conductance between $0.3G_0$ and $10^{-6}G_0$ is below 100 s (see S.I. Figure 3). However, in the presence of backbones **1**, **2**, and **3**, the lifetime of the junction increases significantly (Figure 8 insets), which is a clear signature that a molecule has been trapped between the electrodes. The junction formation probability, calculated as described in the Experimental Section, is different for each anchoring group and

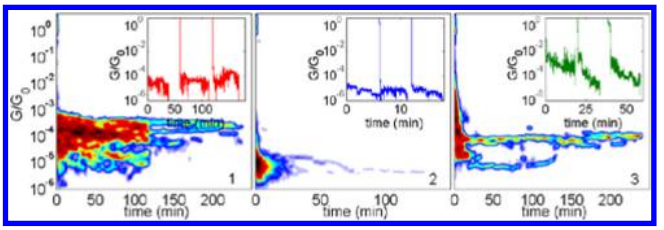

Figure 8. Self-breaking trace histograms obtained from 61, 336, and 139 breaking traces such as those shown in the insets for junctions exposed to 0.5 mM solutions of **1**, **2**, and **3**, respectively. The bias voltage was 0.1 V.

decreases in the order thiols (86%) > pyridines (59%) > acetylenes (39%). Moreover, the average lifetime for each molecule was obtained from the Gaussian fit of the junction lifetime histogram (see S.I. Figure 4). The thiol and pyridine backbones display well-defined peaks at 97 and 3 min, respectively. In the case of acetylenes, the trapping probability is significantly lower, and thus, about 61% of the signal in the lifetime histogram comes from nontrapped molecules. Nevertheless, a peak at a lifetime above 10^4 s (167 min), which corresponds to the lifetime of the plateau visible in the self-breaking trace histogram, can be distinguished.

The 1D conductance histograms constructed from the SB traces in Figure 8 reveal well-defined peaks for all three backbones (Figure 9). Gaussian fits to these peaks were used to

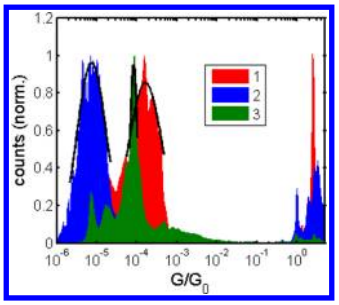

Figure 9. One-dimensional conductance histograms obtained from the measured SB trace histograms of molecular backbones **1**, **2**, and **3** shown in Figure 8. The most probable conductance values were obtained from Gaussian fits of the conductance histograms (black lines).

identify the preferred conductance values of **1** ($1.6 \times 10^{-4}G_0$), **2** ($7.4 \times 10^{-6}G_0$), and **3** ($8.3 \times 10^{-5}G_0$). Comparing these results with those obtained in the previous section using the traditional MCBJ method (Figure 8), we find that the SB method provides narrower single-conductance peaks, even for **3**, for which a particularly well-defined peak was found. In the case of **1**, we passed from a broad peak centered around $2.1 \times 10^{-5}G_0$ to a peak at $1.6 \times 10^{-4}G_0$ with a variance comparable to that of **2**. For backbone **2**, the values obtained with the two methods compare quite well in terms of conductance value and peak width.

*Conductance Histograms of **1c**–**3c** Obtained by the SB Method.* In contrast to the MCBJ experiments, well-defined conductance plateaus could be obtained for compounds **1c**–**3c** using the SB method. Figure 10 shows the conductance histograms obtained from 35, 77, and 52 self-breaking traces for **1c**, **2c**, and **3c**, respectively. In this case, 88, 89, and 100% of the curves displayed lifetimes greater than 100 s with average lifetimes of 31, 7, and 163 min, respectively (see S.I. Figure 4).

dx.doi.org/10.1021/ja5012417 | J. Am. Chem. Soc. XXXX, XXX, XXX–XXX

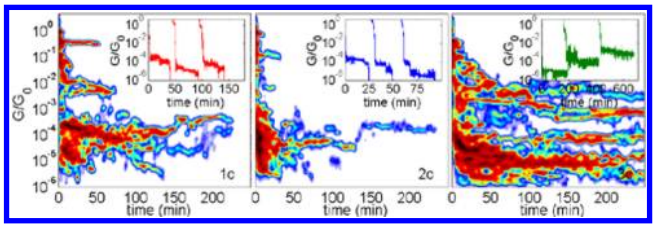

Figure 10. SB trace histograms obtained from 35, 77, and 52 breaking traces such as those shown in the insets for junctions exposed to 0.5 mM solutions of **1c**, **2c**, and **3c**, respectively. The bias voltage was 0.1 V.

In the case of the copper complexes, we found the probability of junction formation obtained by the MCBJ method to be smaller than that obtained by the SB method. We attribute this higher probability for the SB technique to a difference in trapping probability when the electrode displacement speed is varied.[63] Specifically, in **1c**−**3c** the presence of the ring makes the molecule bulkier, and this may hamper the junction formation when the electrodes are quickly displaced. In the SB method, however, the time for junction formation is longer, and thus, the chance of trapping the molecules in between increases. Furthermore, we found that once the complexes **1c**, **2c**, and **3c** were trapped, they remain bonded to the leads for times similar to those of backbones **1**, **2**, and **3**, respectively. These facts suggest that a similar configuration is adopted in the junction and that the complexes are not attached by the ring component. Moreover, the junction average lifetimes are roughly in agreement with the anchor−Au bond strengths according to the sequence Au−C > Au−S ≫ Au−N.[64,65]

The most probable conductance values of copper complexes **1c**−**3c** were extracted from the Gaussian fits of the 1D molecular histograms shown in Figure 11. Comparison with the

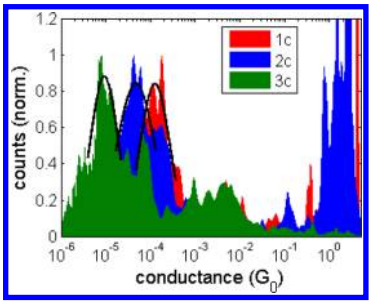

Figure 11. One-dimensional conductance histograms obtained from the measured SB trace histograms of copper complexes **1c**, **2c**, and **3c** shown in Figure 10. The most probable conductance values and their variances were obtained from Gaussian fits of the conductance histograms (black lines).

conductance values obtained for the bare backbones showed the effects of Cu(I) coordination: the conductance of **1c** ($1.3 \times 10^{-4}G_0$) exhibited a subtle decrease with respect to that of **1** ($1.6 \times 10^{-4}G_0$), whereas **2c** ($4.7 \times 10^{-5}G_0$) displayed an increase in conductance by about 1 order of magnitude with respect to backbone **2** ($7.4 \times 10^{-6}G_0$) and **3c** ($9.2 \times 10^{-6}G_0$) displayed a decrease by about 1 order of magnitude with respect to **3** ($8.3 \times 10^{-5}G_0$). These different trends observed for the three types of termination cannot be attributed simply to changes in the HOMO−LUMO gap, since **1**, **2**, and **3** present similar drops in the gap of about 1 eV upon Cu(I) coordination (see Table 1). Therefore, we resorted to theoretical calculations to get a closer look into the energy level alteration induced by copper coordination in the different wires.

NEGF+DFT Calculations. We also performed more realistic NEGF+DFT calculations for the gold devices with backbones **1**−**3** and the Cu(I) complexes **1c**−**3c**. As previously observed in the calculations on the isolated molecules, coordination of Cu(I) results in a general shift of the density of states toward lower energies. Besides, the transmission spectra and molecule-projected densities of states of **1**, **2**, and **3** (see S.I. Figure 5) are in concordance with previous studies on similar molecules[66,67] and indicate that transport in thiol derivative **1** and acetylene derivative **3** is HOMO-dominated, whereas in the pyridine-anchored system **2** the LUMO is the orbital closest to the Fermi energy. The calculated zero-bias conductance indicates that **2c** ($5.7 \times 10^{-4}G_0$) is significantly more conductive than **2** ($2.5 \times 10^{-6}G_0$), whereas **1c** ($3.8 \times 10^{-3}G_0$) and **3c** ($4.0 \times 10^{-4}G_0$) are less conductive than their parent wires **1** ($1.4 \times 10^{-2}G_0$) and **3** ($1.0 \times 10^{-2}G_0$), respectively. These trends are in qualitatively good agreement with the experimentally measured conductances, although a quantitative comparison fails because of the well-known drawback of the generalized gradient approximation functionals in the estimation of the HOMO−LUMO gap due to the presence of the self-interaction error, which leads to an overestimation of the calculated conductance.[68,69]

In summary, experiment and theory agree that for pyridine-ended systems there is a considerable increase of the conductance upon coordination, whereas in the case of thiol- and acetylene-functionalized molecules the molecular conductance decreases upon coordination. This picture can be explained in terms of the alignment between the molecular orbitals and the gold Fermi level. Since the Fermi level of the gold electrodes lies in the HOMO−LUMO gap, the orbital stabilization resulting from the coordination of Cu(I) should bring the LUMO level closer to it, enhancing its contribution to the current. That is the reason why the conductance in pyridines, where the transport is LUMO-mediated, increases upon coordination. By contrast, the shift of the HOMO toward lower energies moves this orbital away from the Fermi level, thereby decreasing the conductivity of the molecular systems in which the transport is HOMO-dominated, that is, the thiol and acetylene derivatives.

■ CONCLUSIONS

We have used the mechanically controlled and SB junction formation techniques to measure the room-temperature low-bias conductance of a family of conjugated ligands and their corresponding Cu(I) complexes. Specifically, we have studied the single-molecule conductance of a family of oligo(arylene phenylene) phen molecular wires functionalized with thiol, pyridine, or acetylene anchoring groups before and after Cu(I) coordination.

The prepared conjugated molecular backbones presented good conductance features, in accordance with those of similar reported systems. By the MCBJ method, the most probable molecular conductance values could be extracted only from the conductance histograms of the thiol and pyridine derivatives. By contrast, acetylene derivatives did not show clearly defined plateaus, and no precise conductance values could be extracted. In all cases, pyridine-ended derivatives afforded very stable and reproducible junctions, confirming that they are an excellent

dx.doi.org/10.1021/ja5012417 | J. Am. Chem. Soc. XXXX, XXX, XXX−XXX

option for charge transport studies. In contrast to the MCBJ method, the SB technique afforded a high junction formation probability for our bulky Cu(I) complexes and turned out to be a very suitable alternative independent of the anchoring group used. These differences between the two techniques are probably related to the different time scales involved in the junction formation.

In regard to the effect of metal coordination, the design of our molecular backbones enabled for the first time an evaluation, at the single-molecule level, of the effect of Cu(I) coordination on the conductance of molecular wires while excluding any contribution from metal-induced conformational changes. As expected, the spectral and electrochemical features of the Cu(I) oligo(arylene phenylene)phenanthroline complexes reflected significantly lower HOMO−LUMO energy gaps than their parent backbones. However, we observed that in contrast to what has been previously reported,[5,6,12,13] metal coordination was not always followed by a molecular conductance enhancement. We studied the energy density of states diagrams for both the ligands and the complex-contacted molecules by NEGF+DFT calculations. In accordance with previous works, in the thiol and acetylene backbones (**1** and **3**) the electron transmission takes place through the HOMO level, whereas in the pyridine system (**2**) the orbital mainly involved in the conduction is the LUMO. The shift of the ligand levels to lower energies induced by the coordination of Cu(I) increases the energy difference between the HOMO and the gold Fermi level, reducing the conductance in the cases of **1c** and particularly **3c**. By contrast, in the case of **2c**, the stabilization of the frontier orbitals reduces the energy difference between the LUMO and the Fermi level, leading to a better level alignment that is reflected in a considerable conductance increase. Consequently, the observed differences in conductance after metal coordination cannot be correlated with the reduction of the HOMO−LUMO gap but instead are correlated with the particular displacement of the molecular levels involved in electron transport with respect to the Fermi level of the electrodes. This shift of the ligand levels toward lower energies is expected to have different magnitudes for various transition-metal ions,[55] and thus, similar trends in the molecular conductance of thiol-, pyridine-, and acetylene-ended conjugated wires are expected for other metals. Furthermore, these results open the door to the study of the conductance response to the redox switching behavior of copper-based interlocked molecules embedded in molecular junctions.[70]

■ ASSOCIATED CONTENT

Supporting Information

Chemical synthesis procedures, spectroscopic and electrochemical data for the compounds, lifetime histograms, and calculated transmission spectra. This material is available free of charge via the Internet at http://pubs.acs.org.

■ AUTHOR INFORMATION

Corresponding Authors

h.s.j.vanderzant@tudelft.nl
eugenio.coronado@uv.es

Author Contributions

⊥J.P. and C.R.A. contributed equally.

Notes

The authors declare no competing financial interest.
This article forms part of the Ph.D. thesis of J.P.

■ ACKNOWLEDGMENTS

The present work was funded by the EU (Project ELFOS, SAMSFERE-321739, and ERC Advanced Grants SPINMOL and Mols@Mols), the Spanish MINECO (Grants MAT2011-22785, MAT2007-61584, and CTQ2011-23862-C02-01 and the CONSOLIDER-INGENIO Project on Molecular Nanoscience), and the Generalidad Valenciana (Prometeo and ISIC Programmes of Excellence). The research reported here was also supported by the Regional Generalitat de Catalunya Authority (2009SGR-1459). J.P and S.T. thank the Spanish MICINN for a predoctoral fellowship and a JdlC postdoctoral contract, respectively. D.A. thanks Conicyt-Chile for a predoctoral fellowship. The authors gratefully acknowledge the computer resources, technical expertise, and assistance provided by the BSC (Siesta calculations) and CESCA (Gaussian calculations).

■ REFERENCES

(1) Tao, N. J. *Nat. Nanotechnol.* **2006**, *1*, 173−181.
(2) Xiao, X.; Brune, D.; He, J.; Lindsay, S.; Gorman, C. B.; Tao, N. *Chem. Phys.* **2006**, *326*, 138−143.
(3) Seo, K.; Konchenko, A. V.; Lee, J.; Gyeong, S. B.; Lee, H. *J. Am. Chem. Soc.* **2008**, *130*, 2553−2559.
(4) Osorio, E. A.; Moth-Poulsen, K.; Van Der Zant, H. S. J.; Paaske, J.; Hedegård, P.; Flensberg, K.; Bendix, J.; Bjørnholm, T. *Nano Lett.* **2010**, *10*, 105−110.
(5) Lee, Y.; Yuan, S.; Sanchez, A.; Yu, L. *Chem. Commun.* **2008**, 247−249.
(6) Lee, Y.; Yuan, S.; Yu, L. *Sci. China: Chem.* **2011**, *54*, 410−414.
(7) Prins, F.; Monrabal-Capilla, M.; Osorio, E. A.; Coronado, E.; Van Der Zant, H. S. J. *Adv. Mater.* **2011**, *23*, 1545−1549.
(8) Mayor, M.; Von Hänisch, C.; Weber, H. B.; Reichert, J.; Beckmann, D. *Angew. Chem., Int. Ed.* **2002**, *41*, 1183−1186.
(9) Park, J.; Pasupathy, A. N.; Goldsmith, J. I.; Chang, C.; Yaish, Y.; Petta, J. R.; Rinkoski, M.; Sethna, J. P.; Abruña, H. D.; McEuen, P. L.; Ralph, D. C. *Nature* **2002**, *417*, 722−725.
(10) Getty, S. A.; Engtrakul, C.; Wang, L.; Liu, R.; Ke, S.-H.; Baranger, H. U.; Yang, W.; Fuhrer, M. S.; Sita, L. R. *Phys. Rev. B* **2005**, *71*, No. 241401(R).
(11) Ruben, M.; Landa, A.; Lörtscher, E.; Riel, H.; Mayor, M.; Görls, H.; Weber, H. B.; Arnold, A.; Evers, F. *Small* **2008**, *4*, 2229−2235.
(12) Xiao, X.; Xu, B.; Tao, N. *Angew. Chem., Int. Ed.* **2004**, *43*, 6148−6152.
(13) Koyama, E.; Naitoh, Y.; Tokuhisa, H.; Nakamura, T.; Horikawa, M.; Ishida, T.; Fujiwara, K.; Mizutani, W.; Nagawa, Y.; Kanesato, M. *Jpn. J. Appl. Phys.* **2008**, *47*, 7369−7371.
(14) Vonlanthen, D.; Mishchenko, A.; Elbing, M.; Neuburger, M.; Wandlowski, T.; Mayor, M. *Angew. Chem., Int. Ed.* **2009**, *48*, 8886−8890.
(15) Mishchenko, A.; Vonlanthen, D.; Meded, V.; Bürkle, M.; Li, C.; Pobelov, I. V.; Bagrets, A.; Viljas, J. K.; Pauly, F.; Evers, F.; Mayor, M.; Wandlowski, T. *Nano Lett.* **2010**, *10*, 156−163.
(16) Venkataraman, L.; Klare, J. E.; Nuckolls, C.; Hybertsen, M. S.; Steigerwald, M. L. *Nature* **2006**, *442*, 904−907.
(17) Hipps, K. W. *Science* **2001**, *294*, 536−537.
(18) Chen, F.; Li, X.; Hihath, J.; Huang, Z.; Tao, N. *J. Am. Chem. Soc.* **2006**, *128*, 15874−15881.
(19) Hong, W.; Manrique, D. Z.; Moreno-García, P.; Gulcur, M.; Mishchenko, A.; Lambert, C. J.; Bryce, M. R.; Wandlowski, T. *J. Am. Chem. Soc.* **2012**, *134*, 2292−2304.
(20) Tour, J. M. *Acc. Chem. Res.* **2000**, *33*, 791−804.
(21) González, M. T.; Leary, E.; García, R.; Verma, P.; Herranz, M. A.; Rubio-Bollinger, G.; Martín, N.; Agraït, N. *J. Phys. Chem. C* **2011**, *115*, 17973−17978.
(22) Tam, E. S.; Parks, J. J.; Shum, W. W.; Zhong, Y. W.; Santiago-Berríos, M. B.; Zheng, X.; Yang, W.; Chan, G. K. L.; Abruña, H. D.; Ralph, D. C. *ACS Nano* **2011**, *5*, 5115−5123.

(23) Li, Z.; Borguet, E. *J. Am. Chem. Soc.* **2012**, *134*, 63−66.
(24) Cheng, Z. L.; Skouta, R.; Vazquez, H.; Widawsky, J. R.; Schneebeli, S.; Chen, W.; Hybertsen, M. S.; Breslow, R.; Venkataraman, L. *Nat. Nanotechnol.* **2011**, *6*, 353−357.
(25) Chen, W.; Widawsky, J. R.; Vázquez, H.; Schneebeli, S. T.; Hybertsen, M. S.; Breslow, R.; Venkataraman, L. *J. Am. Chem. Soc.* **2011**, *133*, 17160−17163.
(26) Hong, W.; Li, H.; Liu, S. X.; Fu, Y.; Li, J.; Kaliginedi, V.; Decurtins, S.; Wandlowski, T. *J. Am. Chem. Soc.* **2012**, *134*, 19425−19431.
(27) Durot, S.; Reviriego, F.; Sauvage, J.-P. *Dalton Trans.* **2010**, *39*, 10557−10570.
(28) Tsutsui, M.; Shoji, K.; Taniguchi, M.; Kawai, T. *Nano Lett.* **2008**, *8*, 345−349.
(29) Fulmer, G. R.; Miller, A. J. M.; Sherden, N. H.; Gottlieb, H. E.; Nudelman, A.; Stoltz, B. M.; Bercaw, J. E.; Goldberg, K. I. *Organometallics* **2010**, *29*, 2176−2179.
(30) Ruthkosky, M.; Castellano, F. N.; Meyer, G. J. *Inorg. Chem.* **1996**, *35*, 6406−6412.
(31) Martin, C. A.; Ding, D.; Van Der Zant, H. S. J.; Van Ruitenbeek, J. M. *New J. Phys.* **2008**, *10*, 1−18.
(32) Rubio-Bollinger, G.; Bahn, S. R.; Agraït, N.; Jacobsen, K. W.; Vieira, S. *Phys. Rev. Lett.* **2001**, *87*, No. 026101.
(33) Becke, A. D. *J. Chem. Phys.* **1993**, *98*, 5648−5652.
(34) Frisch, M. J.; Trucks, G. W.; Schlegel, H. B.; Scuseria, G. E.; Robb, M. A.; Cheeseman, J. R.; Scalmani, G.; Barone, V.; Mennucci, B.; Petersson, G. A.; Nakatsuji, H.; Caricato, M.; Li, X.; Hratchian, H. P.; Izmaylov, A. F.; Bloino, J.; Zheng, G.; Sonnenberg, J. L.; Hada, M.; Ehara, M.; Toyota, K.; Fukuda, R.; Hasegawa, J.; Ishida, M.; Nakajima, T.; Honda, Y.; Kitao, O.; Nakai, H.; Vreven, T.; Montgomery, J. A., Jr.; Peralta, J. E.; Ogliaro, F.; Bearpark, M.; Heyd, J. J.; Brothers, E.; Kudin, K. N.; Staroverov, V. N.; Kobayashi, R.; Normand, J.; Raghavachari, K.; Rendell, A.; Burant, J. C.; Iyengar, S. S.; Tomasi, J.; Cossi, M.; Rega, N.; Millam, N. J.; Klene, M.; Knox, J. E.; Cross, J. B.; Bakken, V.; Adamo, C.; Jaramillo, J.; Gomperts, R.; Stratmann, R. E.; Yazyev, O.; Austin, A. J.; Cammi, R.; Pomelli, C.; Ochterski, J. W.; Martin, R. L.; Morokuma, K.; Zakrzewski, V. G.; Voth, G. A.; Salvador, P.; Dannenberg, J. J.; Dapprich, S.; Daniels, A. D.; Farkas, Ö.; Foresman, J. B.; Ortiz, J. V.; Cioslowski, J.; Fox, D. J. *Gaussian 09*, revision B.01; Gaussian, Inc.: Wallingford, CT, 2009.
(35) Soler, J. M.; Artacho, E.; Gale, J. D.; García, A.; Junquera, J.; Ordejón, P.; Sánchez-Portal, D. *J. Phys.: Condens. Matter* **2002**, *14*, 2745−2779.
(36) Perdew, J. P.; Burke, K.; Ernzerhof, M. *Phys. Rev. Lett.* **1996**, *77*, 3865−3868.
(37) Ma, Z.; Rissner, F.; Wang, L.; Heimel, G.; Li, Q.; Shuai, Z.; Zojer, E. *Phys. Chem. Chem. Phys.* **2011**, *13*, 9747−9760.
(38) Vargas, M. C.; Giannozzi, P.; Selloni, A.; Scoles, G. *J. Phys. Chem. B* **2001**, *105*, 9509−9513.
(39) Hines, T.; Díez-Pérez, I.; Nakamura, H.; Shimazaki, T.; Asai, Y.; Tao, N. *J. Am. Chem. Soc.* **2013**, *135*, 3319−3322.
(40) Ciszek, J. W.; Tour, J. M. *Tetrahedron Lett.* **2004**, *45*, 2801−2803.
(41) Resendiz, M. J. E.; Noveron, J. C.; Disteldorf, H.; Fischer, S.; Stang, P. J. *Org. Lett.* **2004**, *6*, 651−653.
(42) Saitoh, Y.; Koizumi, T.; Osakada, K.; Yamamoto, T. *Can. J. Chem.* **1997**, *75*, 1336−1339.
(43) Ziessel, R.; Suffert, J.; Youinou, M. *J. Org. Chem.* **1996**, *61*, 6535−6546.
(44) Flatt, A. K.; Yao, Y.; Maya, F.; Tour, J. M. *J. Org. Chem.* **2004**, *69*, 1752−1755.
(45) Huang, S.; Tour, J. M. *J. Org. Chem.* **1999**, *64*, 8898−8906.
(46) Dietrich-Buchecker, C. O.; Sauvage, J. P.; Kintzinger, J. P. *Tetrahedron Lett.* **1983**, *24*, 5095−5098.
(47) Schmittel, M.; Michel, C.; Liu, S. X.; Schildbach, D.; Fenske, D. *Eur. J. Inorg. Chem.* **2001**, 1155−1166.
(48) Collin, J.-P.; Gaviña, P.; Sauvage, J.-P. *Chem. Commun.* **1996**, 2005−2006.
(49) Livoreil, A.; Sauvage, J.-P.; Armaroli, N.; Balzani, V.; Flamigni, L.; Ventura, B. *J. Am. Chem. Soc.* **1997**, *119*, 12114−12124.
(50) Armaroli, N. *Chem. Soc. Rev.* **2001**, *30*, 113−124.
(51) Kim, K. Y.; Farley, R. T.; Schanze, K. S. *J. Phys. Chem. B* **2006**, *110*, 17302−17304.
(52) Armaroli, N.; Balzani, V.; Collin, J.-P.; Gaviña, P.; Sauvage, J.-P.; Ventura, B. *J. Am. Chem. Soc.* **1999**, *121*, 4397−4408.
(53) D'Andrade, B. W.; Datta, S.; Forrest, S. R.; Djurovich, P.; Polikarpov, E.; Thompson, M. E. *Org. Electron.* **2005**, *6*, 11−20.
(54) Djurovich, P. I.; Mayo, E. I.; Forrest, S. R.; Thompson, M. E. *Org. Electron.* **2009**, *10*, 515−520.
(55) Manas, E. S.; Chen, L. X. *Chem. Phys. Lett.* **2000**, *331*, 299−307.
(56) Kamenetska, M.; Koentopp, M.; Whalley, A. C.; Park, Y. S.; Steigerwald, M. L.; Nuckolls, C.; Hybertsen, M. S.; Venkataraman, L. *Phys. Rev. Lett.* **2009**, *102*, No. 126803.
(57) Dretschkow, T.; Lampner, D.; Wandlowski, T. *J. Electroanal. Chem.* **1998**, *458*, 121−138.
(58) Pinheiro, L. S.; Temperini, M. L. A. *Appl. Surf. Sci.* **2001**, *171*, 89−100.
(59) Cafe, P. F.; Larsen, A. G.; Yang, W.; Bilic, A.; Blake, I. M.; Crossley, M. J.; Zhang, J.; Wackerbarth, H.; Ulstrup, J.; Reimers, J. R. *J. Phys. Chem. C* **2007**, *111*, 17285−17296.
(60) Lörtscher, E.; Ciszek, J. W.; Tour, J.; Riel, H. *Small* **2006**, *2*, 973−977.
(61) Wang, L. J.; Yong, A.; Zhou, K. G.; Tan, L.; Ye, J.; Wu, G.; Xu, Z.; Zhang, H. L. *Chem.—Asian J.* **2013**, *8*, 1901−1909.
(62) Zhao, X.; Huang, C.; Gulcur, M.; Batsanov, A. S.; Baghernejad, M.; Hong, W.; Bryce, M. R.; Wandlowski, T. *Chem. Mater.* **2013**, *25*, 4340−4347.
(63) González, M. T.; Díaz, A.; Leary, E.; García, R.; Herranz, M. A.; Rubio-Bollinger, G.; Martín, N.; Agraït, N. *J. Am. Chem. Soc.* **2013**, *135*, 5420−5426.
(64) In *CRC Handbook of Chemistry & Physics*, 94th ed.; Haynes, W. M., Ed.; CRC Press: Boca Raton, FL, 2013.
(65) Abdou, H. E.; Mohamed, A. A.; Fackler, J. P. Jr. Gold(I) Nitrogen Chemistry. In *Gold Chemistry: Applications and Future Directions in the Life Sciences*; Mohr, F., Ed.; Wiley-VCH: Weinheim, Germany, 2009; Chapter 1, pp 1−45.
(66) Malen, J. A.; Doak, P.; Baheti, K.; Tilley, T. D.; Segalman, R. A.; Majumdar, A. *Nano Lett.* **2009**, *9*, 1164−1169.
(67) Widawsky, J. R.; Darancet, P.; Neaton, J. B.; Venkataraman, L. *Nano Lett.* **2012**, *12*, 354−358.
(68) Ke, S.-H.; Baranger, H. U.; Yang, W. *J. Chem. Phys.* **2007**, *126*, No. 201102.
(69) Solomon, G. C.; Herrmann, C.; Ratner, M. A. *Top. Curr. Chem.* **2012**, *313*, 1−38.
(70) Coronado, E.; Gaviña, P.; Ponce, J.; Tatay, S. *Chem.—Eur. J.* **2014**, *20*, 6939−6950.